View metadata, citation and similar papers at core.ac.uk

brought to you by CORE

provided by Dadun, University of Navarra

EPJ E
Soft Matter and Biological Physics

EPJ.org
your physics journal

Eur. Phys. J. E (2011) **34**: 133 DOI 10.1140/epje/i2011-11133-5

Stress distribution of faceted particles in a silo after its partial discharge

T. Kanzaki, M. Acevedo, I. Zuriguel, I. Pagonabarraga, D. Maza and R.C. Hidalgo

EDP SCIENCES

Società Italiana di Fisica

Springer

Eur. Phys. J. E (2011) **34**: 133
DOI 10.1140/epje/i2011-11133-5

THE EUROPEAN PHYSICAL JOURNAL E

Regular Article

Stress distribution of faceted particles in a silo after its partial discharge

T. Kanzaki[1,a], M. Acevedo[2], I. Zuriguel[2,b], I. Pagonabarraga[3], D. Maza[2], and R.C. Hidalgo[2,c]

[1] Departament de Física - Universitat de Girona, 17071 Girona, Spain
[2] Departamento de Física, Facultad de Ciencias - Universidad de Navarra, 31080 Pamplona, Spain
[3] Departament de Física Fonamental, Carrer Martí i Franqués, 1, Universitat de Barcelona, 08028 Barcelona, Spain

Received 22 September 2011 and Received in final form 10 November 2011
Published online: 28 December 2011 – © EDP Sciences / Società Italiana di Fisica / Springer-Verlag 2011

Abstract. We present experimental and numerical results of the effect that a partial discharge has on the morphological and micro-mechanical properties of non-spherical, convex particles in a silo. The comparison of the particle orientation after filling the silo and its subsequent partial discharge reveals important shear-induced orientation, which affects stress propagation. For elongated particles, the flow induces an increase in the packing disorder which leads to a reduction of the vertical stress propagation developed during the deposit generated prior to the partial discharge. For square particles, the flow favors particle alignment with the lateral walls promoting a behavior opposite to the one of the elongated particles: vertical force transmission, parallel to gravity, is induced. Hence, for elongated particles the flow developed during the partial discharge of the silo leads to force saturation with depth whereas for squares the flow induces hindering of the force saturation observed during the silo filling.

1 Introduction

Granular materials are ubiquitous in nature and are one of the most manipulated materials in industry. They are very important in applications as diverse as pharmaceutical industry, agriculture, and energy production. Hence, research on these materials is very significant to engineering and physics [1–3]. Despite the relevance of shape in granular materials because of their pervasive nature, most of the theoretical and experimental analysis carried out so far focus on spherical grains. A number of studies performed in recent years have highlighted the qualitatively new features induced by particle shape [4–15] and the new physical scenarios that grain shape gives rise to. These include effects in the packing fraction of granular piles [9,10], the pressure in the lateral walls of a silo during its discharge [11], the mean coordination number [12], the jamming [13] and the stress propagation in granular piles [14,15]. Moreover, there is currently increasing interest on the effect that faceted particles have in the global behavior of granular materials [16–24]. Those systems are common in geomaterials and with high relevance in civil engineering applications [25,26].

The design and exploitation of granular silos benefits from a detailed knowledge of the mechanical properties of particle storages. In fact, a poor understanding of the impact that the grain properties has on granular deposits necessary leads to a poor performance of the silo, both in terms of its storage capabilities as well as its overall structural stability. Since the collective behavior of such systems is not always easy to measure and control experimentally, numerical modeling usually provides a very useful complementary approach for understanding very complex processes like silo filling and discharging [5,11,27–29].

In previous works we have clarified the remarkable role that flat faces play in the stress propagation of granular deposits [22,23]. Elongation favors rods' alignment transverse to gravity, hindering stress transmission to the lateral walls of the container. Then, as the particles increase their length, force saturation becomes strongly reduced. On the contrary, squares tend to orient with a diagonal parallel to gravity, transmitting the stress at $\pi/4$ with respect to the gravity. This results in a clear saturation of the pressure with depth, similar to what is observed in granular silos and known as Janssen's effect.

In this work, we present a systematic theoretical and experimental study of the structural and mechanical properties of packings of faceted particles after their partial discharge from a silo. We show that particle shape and elongation has a profound effect on the process of silo discharge and consequently, on the stress profiles devel-

[a] e-mail: tkanzakic@gmail.com
[b] e-mail: iker@fisica.unav.es
[c] e-mail: raulcruz@unav.es

oped. Hence, grain aspect ratio becomes a key parameter which controls the properties of packings of faceted particles within a silo.

2 Experiment

The experimental setup consists on a smooth, two-dimensional silo filled either with rods or square nuts (fig. 1). Two types of rods of 1.0 mm diameter have been used in this work. Both are monodisperse stainless steel rods with different lengths: 2.4 and 5.4 mm. Hence, the aspect ratio of the rods is $d = 2.4$ and $d = 5.4$. It is important to note that the borders of the rods are truncated cones as explained in [23]. The square particles, $d = 1$, are DIN 557 nuts 3.16 mm wide and 6.9 mm side.

The container is built with two glass plates separated by two stainless-steel strips 0.1 mm thicker than the particles so that the granular material is confined in a monolayer between the plates. The bottom of the silo is flat and formed by two facing metal pieces whose edges touch each other. Since rods and squares have different sizes, we have modified the container dimensions correspondingly to generate analogous deposits. For rods (squares) the silo is 180 mm (260 mm) wide and 790 mm (950 mm) high. The number of rods necessary to fill the silo is larger than 5×10^4 and 2×10^4 for $d = 2.4$ and $d = 5.4$ mm, respectively; while the number of required squares is around 5×10^3.

The granular sample is introduced through a hopper at the top of the silo by pouring the grains homogeneously along the whole silo width. The feed rate is measured to be around 200 particles per second for 2.4 mm rods, around 80 particles per second for 5.4 mm rods, and 70 particles per second for squares. Once the deposit is generated, an orifice is opened at the silo bottom by separating the two metal pieces that conform it. After a layer of rods (squares) of around 250 mm (300 mm) has flowed out of the silo, the outlet is closed and the flow is arrested. Then, the silo is completely emptied before a new realization is performed. The outlet size is chosen to be small enough to stay away from the silo lateral walls but big enough in order to guarantee the particle flow. At this point, we remark that the flat faces of the particles provoke jams much more frequently than in the case of the spheres [30]. Hence, the outlet sizes selected have been 80 mm, 30 mm and 80 mm for square nuts, $d = 2.4$ rods and $d = 5.4$ rods, respectively. In any case, it should be noted that, although these dimensions may slightly affect some of the quantitative values obtained in this work, the qualitative behavior remains unaltered.

A standard 10.2 megapixel camera is used to take pictures of the grains inside the silo both after the filling and after the partial discharge. The region recorded covers the whole width of the silo and a height going from 290 mm to 410 mm for the case of the rods. For the case of the squares, the height covered goes from 270 mm to 440 mm. In both cases we make sure that this region is high enough to avoid the influence of the silo bottom. From the images, the particles are detected and their position and orientation determined. In order to obtain good statistics we have performed 100 realizations for each sample.

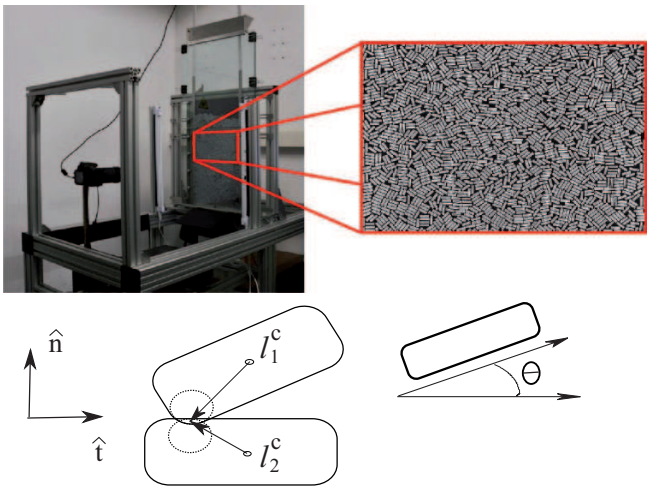

Fig. 1. Photograph of the experimental setup of the two-dimensional silo. On the right, as example, there is a zoom of the $d = 5.4$ rods deposited in the bulk of the granular layer.

3 Model

We have performed a Molecular Dynamics simulation of a two-dimensional granular system composed of non-deformable dissipative particles, confined within a rectangular box of width W. We have simulated 2×10^4 rods of $d = 2.4$ and $d = 5.4$, even so 4×10^3 squares. In order to generate deposits analogous to the experimental ones, the system width is set to $W = 180$ mm ($W = 172.8$ mm) for $d = 2.4$ ($d = 5.4$) and $W = 276$ mm for $d = 1$. The container boundaries are composed of rigid particles, using one layer for each lateral wall, and two particle layers at the bottom.

The particles are continuously added at the top of the box with a low feed rate with random initial velocity and orientation. The granular media is deposited under the effect of gravity and it is let cool down until the particles' mean kinetic energy is several orders of magnitude smaller than its initial value. At this point, a hole of 80 mm, 36 mm and 80 mm for $d = 1$, $d = 2.4$ and $d = 5.4$, respectively, is opened at the middle-bottom of the container. The orifice is closed when a grain located at the top-middle position of the hill, marked as a reference, descends a prescribed vertical distance, s. The distance s takes the value of 300 mm for $d = 1$, 150 mm for $d = 2.4$, and 250 mm for $d = 5.4$. After closing the container we let the system to cool down again and the simulation finishes. To get good statistics, the results presented constitute averages over at least twenty-four different repetitions for each case.

In the simulation, each particle i ($i = 1...N$) has three degrees of freedom, two for the translational motion and

one for the rotational one. The particles' motion is governed by Newton's equations of motion

$$m\ddot{\boldsymbol{r}}_i = \sum_j^c \boldsymbol{F}_{ij} - mg\ \hat{e}_y, \qquad I\ddot{\theta}_i = \sum_j^c (\boldsymbol{l}_{ij} \times \boldsymbol{F}_{ij}) \cdot \hat{e}_z, \quad (1)$$

where m is the mass of particle i, I its momentum of inertia. $\boldsymbol{r}_i$ its position and φ_i its rotation angle. g is the magnitude of the gravitational field and $\hat{e}_y$ is the unit vector along the vertical direction. In eq. (1) $\boldsymbol{F}_{ij}$ accounts for the force exerted by particle j on i and it can be decomposed as $\boldsymbol{F}_{ij} = F_{ij}^N \cdot \hat{n} + F_{ij}^T \cdot \hat{t}$, where F_{ij}^N is the component on the normal direction of the contacting surface $\hat{n}$ (see fig. 1). Complementary, F_{ij}^T is the component acting on the tangential direction $\hat{t}$. For calculating the particles interaction $\boldsymbol{F}_{ij}$ we use a very efficient algorithm proposed recently by Alonso-Marroquín *et al.* [6, 7], allowing for simulating a large number of particles. This numerical method is based on the concept of spheropolygons, where the interaction between two contacting particles only is governed by the overlap distance between them (see details in [6, 7]). For defining the normal interaction F_{ij}^N, we use a nonlinear Hertzian elastic force [31], proportional to the overlap distance of the particles. Moreover, to introduce dissipation, a velocity dependent viscous damping is assumed. Hence, the total normal force reads as

$$F_{ij}^N = -k^N \cdot \delta^{3/2} - \gamma^N \cdot v_{\text{rel}}^N, \quad (2)$$

where k^N is the spring constant in the normal direction, γ^N is the damping coefficient in the normal direction and $\boldsymbol{v}_{\text{rel}}^N$ is the normal relative velocity between i and j. The tangential force F_{ij}^T also contains an elastic term and the tangential frictional term. Taking into account the Coulomb's constraint, it reads as

$$F_{ij}^T = \min\{-k^T \cdot \xi - \gamma^T \cdot |v_{\text{rel}}^T|,\ \mu F_{ij}^N\}, \quad (3)$$

where γ^T is the damping coefficient on the tangential direction, v_{rel}^T is the tangential component of the relative contact velocity of the overlapping pair. ξ represents the elastic elongation of an imaginary spring at the contact [32], which increases as $\mathrm{d}\xi(t)/\mathrm{d}t = v_{\text{rel}}^T$ as long as there is an overlap between the interacting particles [32, 33]. μ accounts for the statical friction coefficient of the particles.

The equations of motion are integrated using a fifth order predictor-corrector algorithm with a numerical error proportional to $(\Delta t)^6$ [34], while the kinematic tangential displacement, is updated using an Euler's method. In order to model hard particles, the maximum overlap must always be much smaller than the particle size. This is ensured by introducing appropriate values for the normal and tangential elastic constants, which are set to $\frac{k_t}{k_n} = 0.1$, $k_n = 10^6\ \mathrm{N/m^{3/2}}$, together with the gravitational acceleration $10\ \mathrm{m/s^2}$. For these parameters, the time step should be around $\Delta t = 5 \times 10^{-5}\mathrm{s}$. Although the results we will describe are generic for hard particles, to achieve quantitative comparison with experimental data we have carried out numerical simulations in which we change both t he normal damping coefficient and the static friction coefficient, choosing the best fitting parameters. The damping coefficients are taken as $\frac{\nu_n}{\nu_t} = 3$, $\nu_t = 1 \times 10^2\ \mathrm{s}^{-1}$ and $\mu = 0.5$. Thus, we have ensured that the kinetic energy loss and the dynamics of sediment formation are analogous to those observed experimentally. It is important to remark that in all the simulations reported below we do not change the particle's material properties; only the particle aspect ratio has been varied.

4 Results

4.1 Packing morphology

In [22,23] we studied systematically the influence that the particle aspect ratio has on the micro-mechanical properties of granular packing. Figure 2 shows the packings obtained for square particles, $d = 1$, both experimentally and numerically. The granular columns resulting from the silo filling process are presented in fig. 2a (exp) and fig. 2c (simul). Figure 2a confirms experimentally the tendency of square particles to align one of their diagonals with gravity, as it was numerically predicted earlier [22].

We also describe in details the morphological and micro-mechanical changes, which are induced by partial discharges in granular columns. The packing morphology that results at the end of the partial discharge of the silo is illustrated in fig. 2b (exp) and fig. 2d (simul). It is noticeable that during the discharge, the shear between grains induces their rotation and their settlement in more stable mechanical states. Hence, the discharge induces an alignment of the squares sides with gravity which minimizes the friction and favors their vertical displacement.

The distributions, $f(\theta)$, of the particle orientation with respect to the direction transverse to gravity are analyzed. Figure 3 shows the particle distributions obtained experimentally and numerically at the end of the silo filling and after the silo partial discharge for three aspect ratios, $d = 5.4, 2.4$, and 1 (squares). The good agreement between the experimental and numerical results demonstrates the accuracy of our numerical simulation scheme. At the end of the silo filling, elongated particles have a strong preference to align horizontally (fig. 3a), in good agreement with previous results [35]. As the rods become less asymmetric, particles develop a most probable orientation which decreases towards $\pi/4$ for the limiting case of squares. In this case, it also becomes evident an important effect of the lateral walls which compete with gravity and lead to a strong preference for parallel ordering of squares in their vicinity. As a result, a distinct peak around $\theta = 0$ and $\theta = \pi/2$ can be also identified in fig. 3c. In sphere packings an analogous wall-induced particle ordering, which can be significant in stress transmission, has been previously reported [36, 37].

The packing morphology drastically changes at the end of the partial discharge of the silo. For the case of rods (fig. 3a-b) the discharge induces a decrease of the number of particles oriented horizontally and an

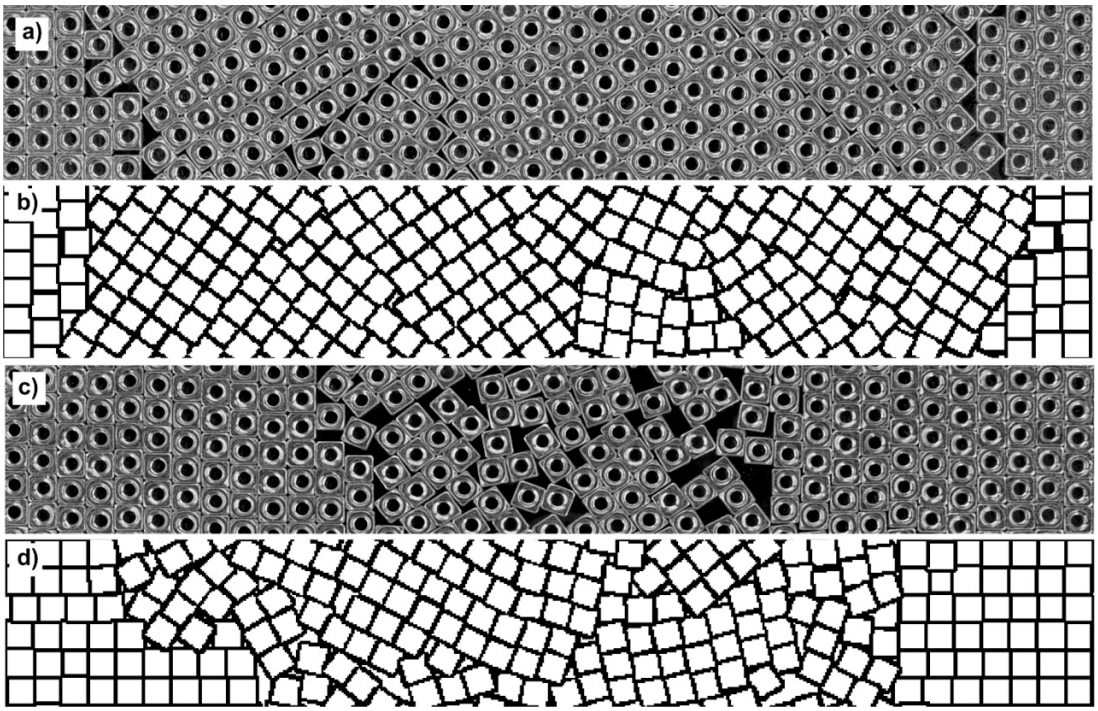

Fig. 2. Packings of square nuts and simulated particles with $d = 1$. Pictures of the experiment (a) after the silo filling and (c) after the partial discharge. Numerical graphs (b) and (d) on the same order.

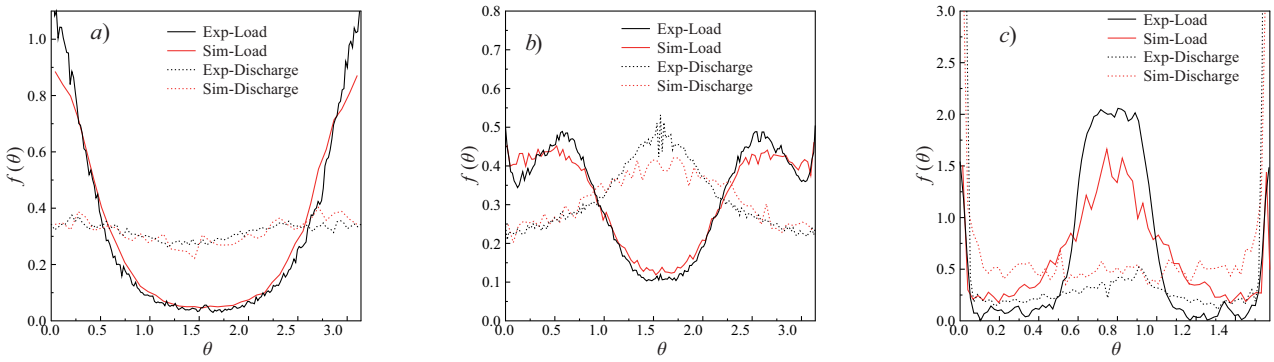

Fig. 3. (Color online) Experimental and numerical orientation distributions of particles, obtained at the end of the silo filling and after its partial discharge. We illustrate results for different aspect ratios: a) $d = 5.4$, b) $d = 2.4$ and c) $d = 1$.

increase of the number of particles oriented vertically. This result may be a consequence of the alignment of elongated particles with the flow streamlines. The case of squares is completely different as it has been observed that they flow more easily when one of their sides is aligned with gravity. This change in the squares orientation, favored due to shearing forces with grains at rest, leads to a distribution where a single peak is clearly observed at $\theta = 0$ and $\theta = \pi/2$ (fig. 3c). We clarify below that this configuration minimizes the friction with the lateral neighboring particles and, consequently, the stress transmission on the up-down direction is favored.

Although in the previous paragraphs we have analyzed the particle orientation distribution by considering all the particles along the whole silo width, it should be remarked that the partial silo discharge induces a spatial inhomogeneity in the horizontal direction. This effect is observed for all the aspect ratios but it is specially dramatic for the case of squares. In fig. 4 we quantify the internal structure analyzing the fraction of square particles which align their side (diagonal) with gravity, at angles $0 < \theta < \pi/8$ and $\theta > \pi - \pi/8$ ($\pi/4 - \pi/8 < \theta < \pi/4 + \pi/8$), as a function to the distance to the left parallel wall of the silo, $P_{\frac{\pi}{2}}(x)$ ($P_{\frac{\pi}{4}}(x)$). At the end of the filling process, most particles align their diagonals with gravity, except for a narrow region close to the walls. After the partial discharge, it is evident that the fraction of squares with a diagonal parallel to gravity is strongly depleted from the wall region, while in the center, both groups of orientations are present with similar probability. This result reflects what is observed

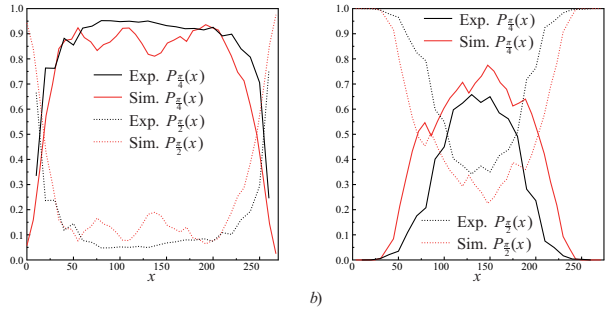

Fig. 4. Experimental and numerical orientation of the squares for different sectors of the silo a) at the end of the silo filling and b) after the silo partial discharge. $P_{\frac{\pi}{2}}(x)$ accounts for the fraction of particles aligned mostly transversally to gravity, while $P_{\frac{\pi}{4}}(x)$ accounts for the fraction of particles mostly aligned with gravity.

by visual inspection of the discharge process: a column of particles, limited by the orifice size, flows out the central part of the silo. In the regions closer to the lateral walls the strong friction between the moving particles and those at rest favors the growth of clusters of squares with their sides aligned with the walls. This kind of flow is known as ratholing, a characteristic and undesirable effect in silo discharge, where stagnant zones are developed near the walls as only the particles above the silo outlet are able to flow out [38].

4.2 Micromechanics

The study of the micromechanical properties of the granular packings will provide more insight in the correlation between the deposit microstructure and stress transmission. We can define the stress acting on a single particle i in terms of $\boldsymbol{F}_i^c$, the force it experiences due to its contact c. The local stress tensor can be calculated as

$$\sigma^i_{\alpha\beta} = \sum_{c=1}^{C_i} l^c_{i,\alpha} F^c_{i,\beta}, \qquad (4)$$

where $\boldsymbol{l}_i^c$ is the branch vector related to the contact c. The sum runs over all contacts of particle i.

Figure 5 displays polar distributions of the stress tensor principal directions obtained for single particles (see eq. (4)). We present results corresponding to columns of rods with $d = 5.4$ (a and b), and squares (c and d), after loading (a and c) and after partial discharging (b and c). The data shown correspond to an area of 100 mm wide at the center of the silo. In each plot, the discontinuous arrows represent the largest (σ_{11}) and smallest (σ_{22}) eigenvalue of the mean stress tensor, within the whole studied area. The size of the arrows is normalized with the size of the smallest eigenvalue. Note that at the end of the silo filling process, the polar distribution for rods $d = 5.4$ displays a strong preference for the transmission parallel to gravity (fig. 5a). On the contrary, for squares, a clear symmetry is found in the distributions of the two stress

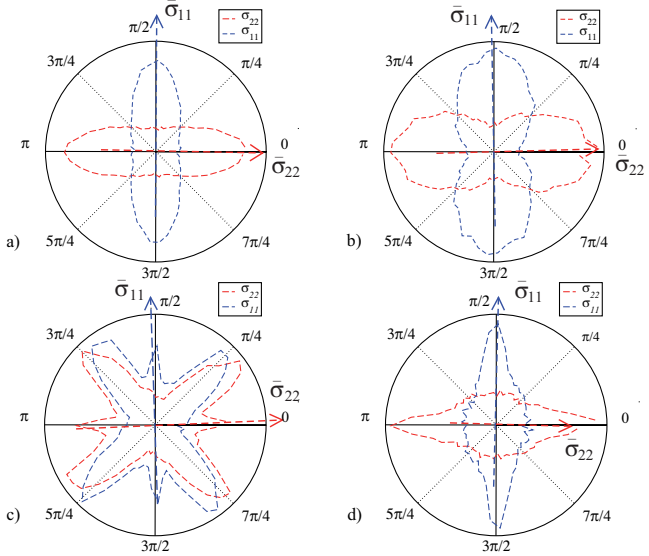

Fig. 5. (Color online) Polar distribution of the principal directions of the *local stress* for elongated particles with aspect ratio $d = 5.4$ (a) after the silo load and (b) after the partial discharge. The same results for squares (c) after the load and (d) after the partial discharge.

eigenvalues, evidencing that forces are mainly transmitted along the $\pi/4$ and $3\pi/4$ directions (fig. 5c). At the end of the partial discharge, elongated rods keep the preference for vertical stress transmission, although the stronger disorder in rod alignment favors a more isotropic stress distribution, leading to broader distributions of the stress eigenvalues (fig. 5b). For the case of the squares, the changes in the stress transmission induced by the particle flow are more important. Indeed, after the partial discharge, the stress changes dramatically and becomes mainly transmitted vertically (fig. 5d). This effect correlates with the formation of big clusters of square particles aligned with the walls. Hence, changes in the particle orientation induced by the shear affect the microstructure and determine the stress transmission among the faceted particles.

The notable changes in the local stress produced by the partial discharge of the silo necessary lead to significant variations in the pressure profiles obtained as a function of the silo depth (h). To properly describe these variations, we examined the mean local stress tensor through the granular column. Professor Isaac Goldhirsch and coworkers [39,40] have recently introduced a very elaborated definition of mean stress field $\bar{\sigma}_{\alpha\beta}$. Following their approach the stress $\sigma_{\alpha\beta}(\boldsymbol{r})$ at point $\boldsymbol{r}$, is given by the expression

$$\bar{\sigma}_{\alpha\beta}(\boldsymbol{r}) = \frac{1}{2} \sum_{i,j;i\neq j} f_{ij\alpha} r_{ij\beta} \int_0^1 \mathrm{d}s\, \phi[\boldsymbol{r} - \boldsymbol{r}_i + s\boldsymbol{r}_{ij}], \qquad (5)$$

where the sum runs over all the contacting particles i, j, whose center of mass are at $\boldsymbol{r}_i$ and $\boldsymbol{r}_j$, respectively. Moreover, $\boldsymbol{f}_{ij}$ accounts for the force exerted by particle j on particle i and $\boldsymbol{r}_{ij} \equiv \boldsymbol{r}_i - \boldsymbol{r}_j$. The coarse-grained (CG) function, $\phi(\boldsymbol{R})$, is positive semidefinite normalized function,

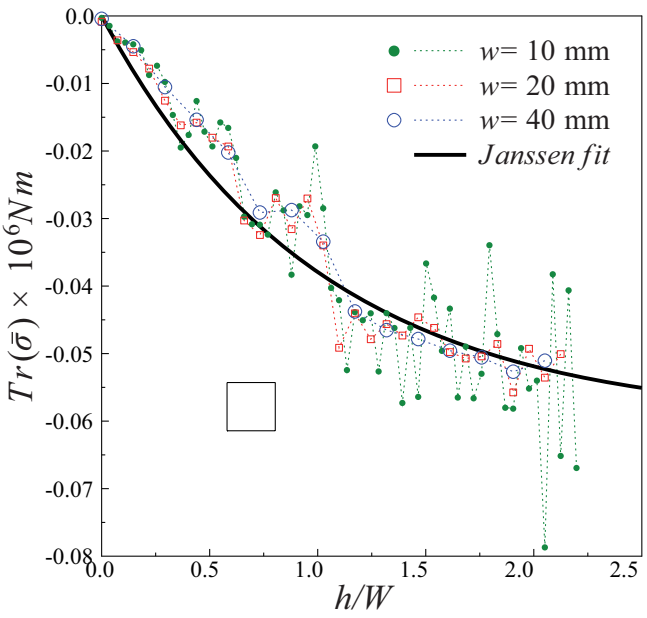

Fig. 6. (Color online) Profiles of the trace of the mean stress tensor, defined following eq. (5), after the silo loading. The results have been obtained using a Gaussian coarse-grained function, $\phi(\boldsymbol{r}) = \frac{1}{\pi w^2} e^{-(|\boldsymbol{r}|/w)^2}$ and several values of w. In all cases the depth h is expressed in units of the silo width. We also show the Janssen-type fitting to the equation $\sigma = \sigma_m(1 - \exp(-x/h_s))$, we have used ($\sigma_m = -0.06 \times 10^6$ N m; $h_s = 1.0$).

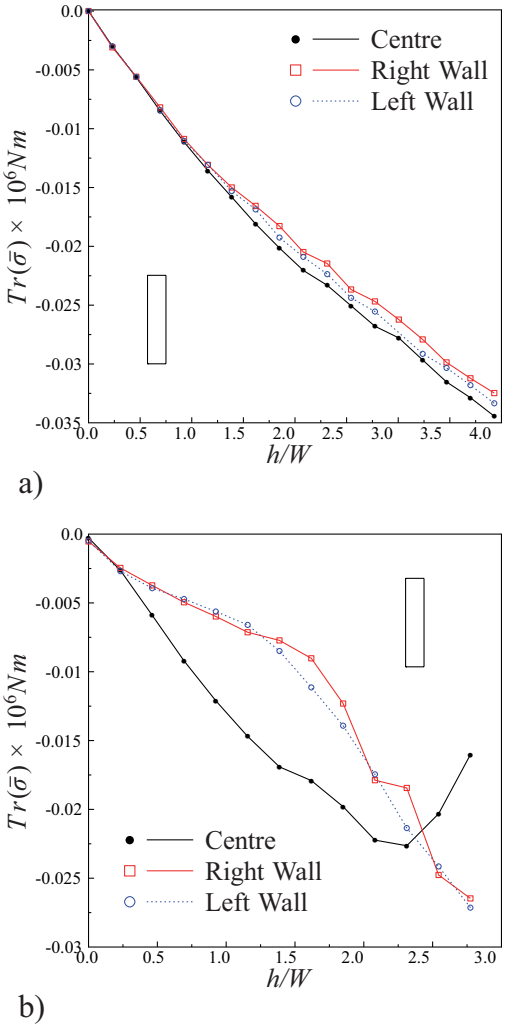

Fig. 7. Profiles of the trace of the mean stress tensor (pressure) after the load a) and the partial discharge b) for rods with $d = 5.4$. In all cases the depth h is expressed in units of the silo width.

with a single maximum at $\boldsymbol{R} = 0$. In our case, we used a Gaussian coarse function, $\phi(\boldsymbol{r}) = \frac{1}{\pi w^2} e^{-(|\boldsymbol{r}|/w)^2}$, where the sign convention is that compressive stress is negative. The value of w defines the coarse-grained scale. We note that the data was also evaluated using less sophisticated mean stress definitions [41,42] and very similar results came out (data not shown).

To clarify the effect of the CG scale w on the results, we evaluate the numerical data for several values of w. The stress tensor components —defined by eq. (5)— were calculated within specific areas and the contribution of the contacts within the selected area is weighted by the function $\phi(\boldsymbol{r})$. Hence, the size of the working area is controlled by the size of the CG scale w. Specifically, the trace of stress tensor (pressure) obtained for a silo of squares was examined in fig. 6. Note that the depth of the silo has been normalized with the width of the deposit $x = h/W$. Moreover, for comparison, the numerical fit using a *Janssen-type* formula $\sigma = \sigma_m(1-\exp(-x/h_s))$, are also shown [43].

Here, the magnitude of σ_m represents the saturation stress and h_s indicates the characteristic value of depth at which the pressure on the column surface stabilizes. The pressure profiles were calculated fixing the horizontal coordinate and varying the vertical one (up-down) in units of w. The results reveal that stress fluctuations at fixed *depth* vanish when increasing the value of w. This indicates the existence of a CG scale for which the stress tensor field is resolution independent [39, 40]. The data presented below have been carefully evaluated for different values of w. Provided that the stress profiles are not homogeneous due to the action of the gravity field, we have carefully chosen the value of w to accurately capture the spatial stress variation.

In fig. 7 and fig. 8, we display the trace of the mean stress tensor for rods $d = 5.4$ and squares, respectively. In all cases, a coarse-grained distance of $w = 40$ mm was used for the calculation of the mean stress tensor. This value is approximately six and seven times larger than particle size of the squares and the rods of $d = 5.4$, respectively. As we pointed out earlier, after the silo loading with elongated particles, the stress is transmitted preferentially parallel to gravity. As a result, the weak stress transmission on the horizontal direction hinders pressure saturation, which is not completely reached for the system sizes studied here (fig. 7a). The pressure profiles are very similar both in the

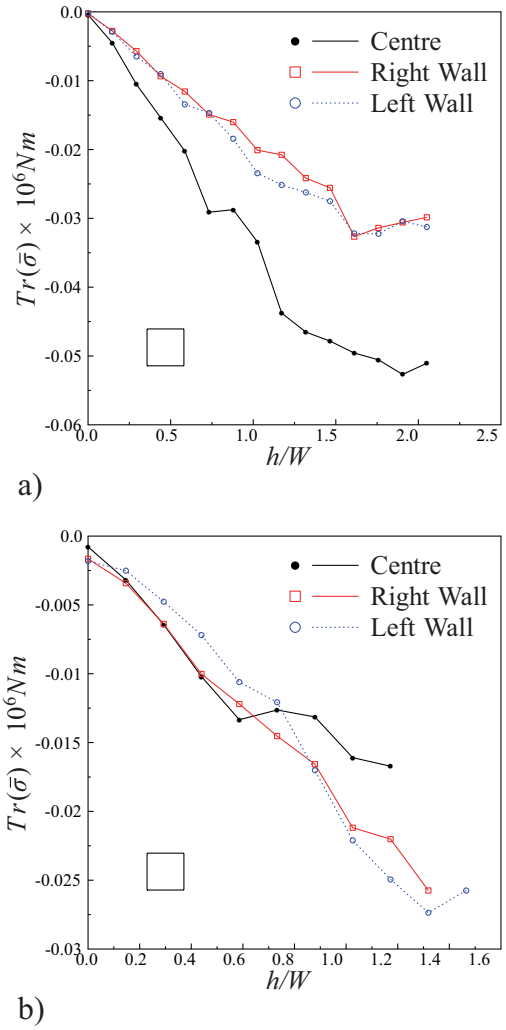

Fig. 8. Profiles of the trace of the mean stress tensor (pressure) after the load a) and the partial discharge b) for squares. In all cases the depth h is expressed in units of the silo width.

center of the column and in the region close to the walls. After the partial discharge (fig. 7b), notable modifications are induced on the trace of the mean stress tensor. On the center of the silo, the larger disorder in particle orientation enhances the stress transmission in the horizontal direction which is typically associated to pressure saturation. Effectively, when we approach to the bottom of the silo the pressure first reaches a maximum and then, it decreases at the very bottom. This pressure reduction denotes arch formation in the region near the outlet. In the region close to the walls the pressure increases with h until the bottom of the silo, probably due to horizontal rod alignment induced by the bottom.

For squares (fig. 8a), the opposite scenario holds true. After filling the silo, in the central part of the column the force is transmitted preferentially at $\pi/4$ with respect to gravity, providing an efficient mechanism to channel stresses towards the lateral walls. Accordingly, a saturation in the pressure profile seems to be observed. However, close to the walls the strong face-to-face interaction induces the particle alignment and, consequently, a linear pressure profile is developed. The scenario is altered by the discharge of the square nuts which become preferentially aligned with the silo walls even in the center part of the column. This vertical alignment results in a stress transfer to the bottom of the silo which makes pressure saturation hardly visible.

Conclusions

In this work we have shown that the partial discharge of a silo filled with faceted grains has a profound effect on the deposit morphology and its stress distribution. During the discharge, the shear between grains induces their rotation and their settlement in more disordered arrangements. For elongated particles, the preferred horizontal orientation displayed after the silo filling disappears. For square particles, the discharge provokes an alignment of their sides with gravity which minimizes the friction and favors their vertical displacement. Such a structure leads to ratholing, a flow pattern which is typically associated to cohesive effects, but that here, we show that it can also be induced by the geometrical properties of the particles.

As a result of the changes in particle orientation, the pressure distribution in the silo changes qualitatively; while for elongated rods lateral stress transmission is promoted by the enhanced disorder leading to a faster pressure saturation, the opposite holds for squares. In this latter case the alignment of squares induced by the flow destroys the initial force chain network which is replaced by a mainly vertical stress transmission. As a consequence, a significant reduction of the pressure saturation effect is observed.

With the results reported here, we attempt to clarify the performance and stability of silos, which need to support high stresses that become very sensitive to grain shapes and the silo steering history. If we increase the amount of material flowing out of the silo, or induce a second discharge, we expect that the observed effect will be enhanced. Although we have focused on weakly disordered initial deposits, due to the low feeding rates used to fill the silo, the main features discussed here are expected for other silo filling procedures. Perhaps, increasing the disorder of the initial packing will generically decrease the relative magnitude of the changes discussed.

The Spanish MICINN (Projects FIS2008-06034-C02-01, FIS2008-06034-C02-02 and FIS2008-04386) and the University of Navarra (PIUNA Program) have supported this work. RCH also acknowledges the financial support of the Spanish MICINN, through a *Ramón y Cajal Program*. TK acknowledge the University of Girona (Spain) for financial support. MA thanks Asociación de Amigos de la Universidad de Navarra for a scholarship. IP acknowledges DURSI (SGR2009-634) for financial support.

References

1. T. Pöschel, T. Schwager, *Computational Granular Dynamics* (Springer-Verlag, Berlin, Heidelberg, New York, 2005).
2. H.M. Jaeger, S.R. Nagel, R.P. Behringer, Rev. Mod. Phys. **68**, 1259 (1996).
3. I.S. Aranson, L.S. Tsimringy, Rev. Mod. Phys. **78**, 641 (2006).
4. J.A.C. Gallas, S. Sokolowski, Int. J. Mod. Phys. B **7**, 2037 (1993).
5. P.W. Cleary, M.L. Sawley, Appl. Math. Modell. **6**, 89 (2001).
6. F. Alonso-Marroquín, H.B. Muhlhaus, H.J. Hermann, Particuology **6**, 390 (2008).
7. F. Alonso-Marroquín, Y. Wang, Granular Matter **11**, 317 (2009).
8. S.A. Galindo-Torres, F. Alonso-Marroquín, Y.C. Wang, D. Pedroso J.D. Muñoz Castaño, Phys. Rev. E **79**, 060301 (2009).
9. F.X. Villarruel, B.E. Lauderdale, D.M. Mueth, H.M. Jaeger, Phys. Rev. E **61**, 6914 (2000).
10. A. Donev, I. Cisse, D. Sachs, E.A. Variano, F.H. Stillinger, R. Connelly, S. Torquato, P.M. Chaikin, Science **303**, 990 (2004).
11. Z. Zhong, J.Y. Ooi, J.M. Rotter, Eng. Struct. **23**, 756 (2001).
12. J. Blouwolff, S. Fraden, EPL **76**, 1095 (2006).
13. K. Desmond, S.V. Franklin, Phys. Rev. E. **73**, 031306 (2006).
14. I. Zuriguel, T. Mullin, J.M. Rotter, Phys. Rev. Lett. **98**, 028001 (2007).
15. I. Zuriguel, T. Mullin, Proc. R. Soc. London, Ser. A **464**, 99 (2008).
16. Vijay Narayan, Narayanan Menon, Sriram Ramaswamy, J. Stat. Mech., P01005 (2006).
17. G. Lumay, N. Vandewalle, Phys. Rev. E **70**, 051314 (2004).
18. G. Lumay, N. Vandewalle, Phys. Rev. E **74**, 021301 (2006).
19. E. Azéma, F. Radjai, R. Peyroux, Phys. Rev. E **76**, 011301 (2007).
20. E. Azéma, F. Radjai, G. Saussine, Mech. Mater. **41**, 729 (2009).
21. E. Azéma, F. Radjai, Phys. Rev. E **81**, 051304 (2010).
22. R.C. Hidalgo, I. Zuriguel, D. Maza, I. Pagonabarraga, Phys. Rev. Lett. **103**, 118001 (2009).
23. R.C Hidalgo, I. Zuriguel, D. Maza, I. Pagonabarraga, J. Stat. Mech., P06025 (2010).
24. T. Kanzaki, R.C. Hidalgo, D. Maza, I. Pagonabarraga, J. Stat. Mech., P06020 (2010).
25. C. Nouguier-Lehon, B. Cambou, E. Vincens, Int. J. Numer. Anal. Meth. Geomech. **27**, 1207 (2003).
26. R.L. Brown, J.C. Richards, *Principles of powder mechanics: essays on the packing and flow of powders and bulk solids* (Pergamon Press, 1970).
27. P.A. Langston, U. Tuzun, D.M. Heyes, Chem. Engin. Sci. **50**, 967 (1995).
28. J.M. Rotter, J.M.F.G. Holst, J.Y. Ooi, A.M. Sanad, Philos. Trans.: Math., Phys. Eng. Sci. **356**, 2685 (1998).
29. M. Guaita, A. Couto, F. Ayuga, Biosyst. Engin. **85**, 101 (2003).
30. A. Janda, I. Zuriguel, A. Garcimartín, L.A. Pugnaloni, D. Maza, EPL **84**, 44002 (2008).
31. L.D. Landau, E.M. Lifshitz, *Theory of Elasticity* (Butterworth-Heinemann, 1986).
32. P.A. Cundall, O.D.L. Strack, Géotechnique **29**, 47 (1979).
33. G. Duvaut, J.-L. Lions, *Les Inéquations en Mécanique et en Physique* (Dunod, Paris, 1972).
34. M.P. Allen, D.J. Tildesley, *Computer Simulation of Liquids* (Clarendon Press, Oxford, 1987).
35. K. Stokely, A. Diacou, S.V. Franklin, Phys. Rev. E. **67**, 051302 (2003).
36. I. Bartos, I.M. Janosi, Granular Matter **9**, 81 (2007).
37. I. Zuriguel, T. Mullin, A. Arevalo, Phys. Rev. E. **77**, 061307 (2008).
38. D. Schulze, *Powders and Bulk Solids. Behaviour, Characterization, Storage and Flow* (Springer-Verlag, Berlin, Heidelberg, 2008).
39. B.J. Glasser, I. Goldhirsch, Phys. Fluids **13**, 407 (2001).
40. I. Goldhirsch, C. Goldenberg, Eur. Phys. J. E **9**, 245 (2002).
41. M. Lätzel, S. Luding, H.J. Herrmann, Granular Matter **2**, 123 (2000).
42. M. Madadi, O. Tsoungui, M. Lätzel, S. Luding, Int. J. Solid Struct. **41**, 2563 (2004).
43. H. A. Janssen, Z. Vereines Deutsch. Ingen. **39**, 1045 (1895).